International Journal of Thermophysics, Vol. 27, No. 2, March 2006 (© 2006)
DOI: 10.1007/s10765-006-0046-1

Interplay Between Wetting and Phase Behavior in Binary Polymer Films and Wedges: Monte Carlo Simulations and Mean Field Calculations[1]

Marcus Müller[2,3] and Kurt Binder[4]

Confining a binary mixture, one can profoundly alter its miscibility behavior. The qualitative features of miscibility in confined geometry are rather universal and shared by polymer mixtures as well as small molecules, but the unmixing transition in the bulk and the wetting transition are typically well separated in polymer blends. The interplay between wetting and miscibility of a symmetric polymer mixture via large-scale Monte Carlo simulations in the framework of the bond fluctuation model and via numerical self–consistent field calculations is studied. The film surfaces interact with the monomers via short ranged potentials, and the wetting transition of the semi–infinite system is of first order. It can be accurately located in the simulations by measuring the surface and interface tensions and using Young's equation. If both surfaces in a film attract the same component, capillary condensation occurs and the critical point is close to the critical point of the bulk. If surfaces attract different components, an interface localization/delocalization occurs which gives rise to phase diagrams with two critical points in the vicinity of the pre-wetting critical point of the semi–infinite system. The crossover between these two types of phase diagrams as a function of the surface field asymmetry is studied. The dependence of the phase diagram on the film thickness Δ for antisymmetric surface fields is investigated. Upon decreasing the film thickness, the two critical points approach the symmetry axis of the phase diagram, and below a certain thickness Δ_{tri}, there remains only a single critical point at the symmetric composition. This corresponds to a second-order interface localization/delocalization transition even though the

[1]Invited paper presented at the Fifteenth Symposium on Thermophysical Properties, June 22–27, 2003, Boulder, Colorado, U.S.A.

[2]Institut für Theoretische Physik, Georg-August-Universität, D-37077 Göttingen, Germany.
[3]To whom correspondence should be addressed. E-mail: mmueller@theorie.physik.uni-goettingen.de
[4]Institut für Physik, WA331, Johannes Gutenberg Universität, D-55099 Mainz, Germany.

wetting transition is of first order. At a specific film thickness, Δ_{tri}, tricritical behavior is found. The behavior of antisymmetric films is compared with the phase behavior in an antisymmetric double wedge. While the former is the analog of the wetting transition of a planar surface, the latter is related to the filling behavior of a single wedge. Evidence for a second-order interface localization/delocalization transition in an antisymmetric double wedge is presented, and its unconventional critical behavior is related to the predictions of Parry *et al.* (*Phys. Rev. Lett.* **83**:5535 (1999)) for wedge filling. The critical behavior differs from the Ising universality class and is characterized by strong anisotropic fluctuations.

KEY WORDS: confined geometry; finite size scaling; Monte Carlo simulation; phase diagram; self-consistent field theory

1. INTRODUCTION

Confining a binary mixture, one can profoundly alter its miscibility behavior [1–4]. The phase behavior of AB mixtures in pores, slits, and films has attracted abiding interest from both theorists and experimentalists [5–7]. We study the interplay between (pre)wetting and phase behavior by self-consistent field (SCF) theory [8,9] and Monte Carlo simulations [10–12]. Particularly, we focus on situations where surfaces attract different components of the mixture.

The qualitative features of the miscibility in confined geometry are rather universal and shared by polymer mixtures as well as small molecules. Symmetric binary polymer blends are, however, particularly well suited to study the interplay between wetting and miscibility: (i) the wetting transition temperature typically is much lower than the critical temperature, where demixing occurs in the bulk [10] and (ii) fluctuations can be controlled by the degree of interdigitation [9,13]: the more extended the molecule is, the larger is the number of neighbors it interacts with, and the smaller is the effect of fluctuations. Therefore, SCF calculations provide an accurate description for many properties except for the ultimate vicinity of critical points. The spatial extension of the molecules also sets the length scale of enrichment layers and facilitates experimental investigations. (iii) The vapor pressure of polymer films is vanishingly small; hence, effects of evaporation can be neglected. (iv) Polymers tend not to crystallize easily. Therefore, wetting phenomena might not be preempted by crystal phases. The blend components have to be liquid and must not arrest in a glassy state. These criteria can be met by experimental systems, and wetting transitions in polymer blends have been studied in recent experiments [6,7]. Likewise, there is no roughening transition of the interface as it occurs in Ising-like models.

Using a coarse-grained polymer [13,14] model for an AB binary melt, we locate the first-order wetting transition, the phase diagram in a symmetric slit pore (symmetric film) [10], and the phase diagram in a thin film where the substrate favors the A-component of the mixture with the same strength as the top surface attracts the B-component (antisymmetric film) [9,11]. Then we discuss the phase behavior in a quadratic pore where two neighboring surfaces favor the A-component and the other two neighboring surfaces favor the B-component (antisymmetric double wedge) [15,16]. We conclude with an outlook.

2. MODEL AND TECHNIQUES

We consider a binary polymer blend. Both species – A and B – contain the same number N of monomers and have the same spatial extension R_e. They are confined into a thin film; the bottom substrate (W) might be a silicon wafer, while the other surface might be the interface to the vapor (vacuum, V). Depending on the ratio between the interface tension γ_{AB} between the segregated bulk phases and the surface tension γ_{AV}, γ_{BV} of the components and the vapor, the upper surface might not be perfectly flat but its shape is dictated by the balance of interface and surface tensions. The qualitative behavior is illustrated in Fig. 1. If the AB interface tension is comparable to the liquid/vapor tension, it "drags" the film surface towards the substrate so as to reduce the length of the AB interface. If the liquid/vapor tension exceeds the AB interface tension by about two orders of magnitude, however, the surface is almost flat and the situation is equivalent to a binary mixture between two hard walls a distance Δ apart [17]. In the following we shall restrict ourselves to this limit $\gamma_{AB} \ll \gamma_{AV}$ or γ_{BV}.

In the Monte Carlo simulations we use a computationally efficient, coarse-grained lattice model. The bond fluctuation model [13,14] retains the universal features of polymers – connectivity, excluded volume of segments, and a thermal interaction which leads to phase separation – but ignores details of chemical structure. Effective monomers prevent the corners of a unit cell of a 3D cubic lattice from double occupancy. We use chain length $N = 32$ and $R_e \approx 17u$. Monomers along a chain are connected via bond vectors of length $2, \sqrt{5}, \sqrt{6}, 3$, or $\sqrt{10}$ in units of the lattice spacing u. Different monomers repel each other by a square-well potential of depth ϵ which comprises the nearest 54 neighbors, like monomers attract each other. The strength of the repulsion is proportional to the Flory–Huggins parameter $\chi = 5.3\epsilon/(k_B T)$ [13]. Surfaces are structureless and impenetrable. They act on monomers in the two nearest layers ($d_{\text{wall}} = 2$) with strength ϵ_{wall}. The range, d_{wall}, of the monomer–surface

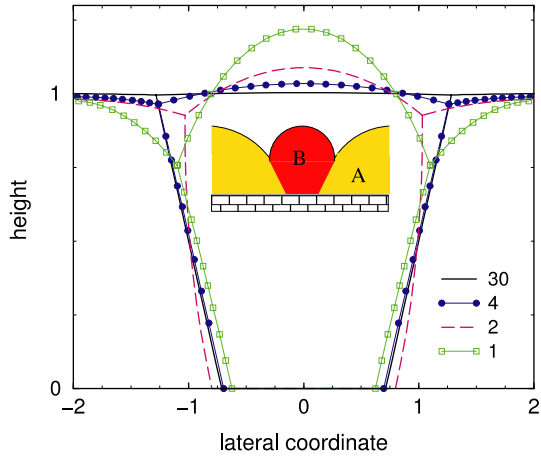

Fig. 1. Laterally segregated binary film. The shape of interfaces is obtained by minimizing the effective Hamiltonian $H = \gamma_{AB}L_{AB} + \gamma_{AS}L_{AS} + \gamma_{BS}L_{BS} + \gamma_{AV}L_{AV} + \gamma_{BV}L_{BV}$ at fixed volume of the components. L_{ij} denotes the length of the interface between substances i and j, and γ_{ij} the corresponding interface tension. $\gamma_{AV} - \gamma_{BV} = \gamma_{AS} - \gamma_{BS} = 0.5\gamma_{AB}$, $\gamma_{BS} = \gamma_{AB}$ and γ_{AV}/γ_{AB} as indicated in the key from Ref. [17].

potential is chosen such that $d_{\text{wall}} \approx \int_0^{d_{\text{wall}}} \mathrm{d}z\ \Phi(z)/\Phi_{\text{bulk}}$ where $\Phi(z)$ denotes the monomer density profile in the z-direction perpendicular to the substrate. Note that $\Phi(z)$ exhibits strong layering effects in the vicinity of the surface because the sizes of the monomers and vacancies differ.

In the SCF calculations we model the polymers as Gaussian chains [8,9,18]. The repulsion between different species is quantified by the Flory-Huggins parameter χ. Short-ranged interactions of strength Λ_1 and Λ_2 attract (repel) the A (B) component in the vicinity of the surfaces, $\Lambda_1 = -\Lambda_2 \approx \frac{\epsilon_{\text{wall}} d_{\text{wall}}}{k_B T R_e}$. The total density profile of the film is imposed. It smoothly decays to zero at the surfaces in a boundary region of width $0.15R_e$. The blend is assumed to be incompressible. This standard Gaussian chain model is solved within the mean-field approximation.

3. WETTING TRANSITION

To accurately locate the wetting transition and calculate the contact angle of macroscopic A-drops we use Young's equation [19] $\gamma_{AB}\cos\Theta = \gamma_{WB} - \gamma_{WA}$. Computationally, this technique [10,20] has distinct advantages for locating first-order wetting transitions: (i) The interface free energy

γ_{AB} and the difference $\Delta\gamma = \gamma_{WB} - \gamma_{WA}$ can be measured accurately in separate simulations thereby avoiding the need for huge simulation cells to simulate a thick A-layer at the surface in equilibrium with a B-rich bulk. (ii) Unlike observing the dependence of the thickness of the A-layer on temperature or monomer-surface attraction, one directly measures free energies. Therefore, we do accurately locate the transition, while the instability of the A-rich layer is located between the transition and the mean-field wetting spinodal. (iii) By virtue of the $A \leftrightharpoons B$ symmetry, the difference $\Delta\gamma$ can also be rewritten as the difference $\Delta\gamma = \gamma_{WB} - \gamma_{-WB}$ of surface tensions of a wall that attract the A-component and a wall that attracts the B-component. This free energy difference can be measured by thermodynamic integration or expanded ensemble methods [10].

The results for our model are presented in Fig. 2. From the crossing of $\gamma_{AB}(\epsilon)$ and $\Delta\gamma(\epsilon)$, we locate the wetting transition. The fact that curves intersect under a finite angle indicates that the wetting transitions are of first order. As we reduce the monomer-surface attraction, the wetting transition shifts to higher temperatures $k_B T/\epsilon$ and become weaker. For all incompatibilities studied, however, the wetting transition is of first order. This is also corroborated by SCF calculations [9,21], where we find first-order wetting transitions for $T/T_c < 0.98$.

If the wetting transition is of first order, then there will be only a small A-rich layer in the non-wet state. By virtue of the structural symmetry of the molecules, they lose the same amount of entropy as they pack against the surface. The surface free energy difference $\Delta\gamma$ is mainly enthalpic. If we assume that the wetting transition is strongly first order, we can neglect the microscopic enrichment layer at the surface. Within this approximation the surface compositions in the non-wet state and the wet state are $\Phi(z=0) \approx 0$ and 1, respectively, and we obtain $\Delta\gamma = 2\epsilon_{\text{wall}} d_{\text{wall}} \Phi$, where $d_{\text{wall}} = 2$ denotes the range of the monomer-surface interaction and $\Phi = 1/16$ is the monomer number density. Using the expression for the interface tension $\gamma_{AB} = \Phi b \sqrt{\chi/6}$ ($b = 3.05$: statistical segment length) in the strong segregation limit [22], we obtain $\chi_{\text{wet}} = 24 \left(\frac{\epsilon_{\text{wet}} d_{\text{wet}}}{b k_B T} \right)^2$.

This is in marked contrast to the value of the Flory–Huggins parameter at the unmixing transition in the bulk, $\chi_c = 2/N \sim 1/T_c$. As both the interface tension γ_{AB} and the difference in surface tension $\Delta\gamma$ are chain-length independent, so is the wetting transition temperature. The fact that the interface and surface tensions are independent from the chain length is also observed in experiments in the limit of long chain lengths. The critical temperature T_c of phase separation, however, increases linearly with chain length N. Therefore, critical phenomena associated with the bulk unmixing and wetting phenomena are well separated.

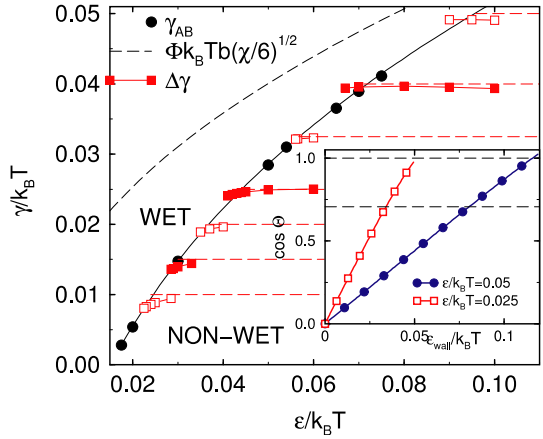

Fig. 2. Interface tension γ_{AB} and difference in surface tensions $\Delta\gamma$ as a function of inverse temperature $\epsilon/(k_BT)$ obtained from simulations. Approximations for the interface tension $\gamma_{AB} = b\Phi\sqrt{\chi/6}$ and $\Delta\gamma = 2\Phi d_{\text{wall}}\epsilon_{\text{wall}} = \epsilon_{\text{wall}}/4$ in the strong segregation limit are also shown. [from Ref. [10]] The inset shows the dependence of the contact angle on ϵ_{wall} for the two temperatures investigated in Section 5.

4. THIN FILMS

4.1. Capillary Condensation and Interface Localization/Delocalization

If the mixture is confined into a film, the surface interactions modify the phase behavior. As wetting is associated with the growth of an infinitely large enrichment layer, it is rounded-off in a thin film [4]. If the wetting transition is of first order, there will be a pre-wetting transition [1]: a coexistence between a thin and thick (but microscopic) enrichment layer at a chemical potential which differs from the value at coexistence in the bulk. As pre-wetting transitions involve only enrichment layers of finite thickness, they might give rise to transitions in thin films.

First we consider a film with symmetric surfaces [10,12], i.e., both surfaces attract the A component. The phase diagram as obtained from the simulations is presented in Fig. 3. Compared to the phase behavior in the bulk, the critical point is shifted to lower temperatures and larger composition of the species attracted by the surfaces. Moreover, the binodals in the vicinity of the critical points exhibit two-dimensional (2D) Ising critical behavior in contrast to the 3D Ising behavior of the bulk unmixing transition.

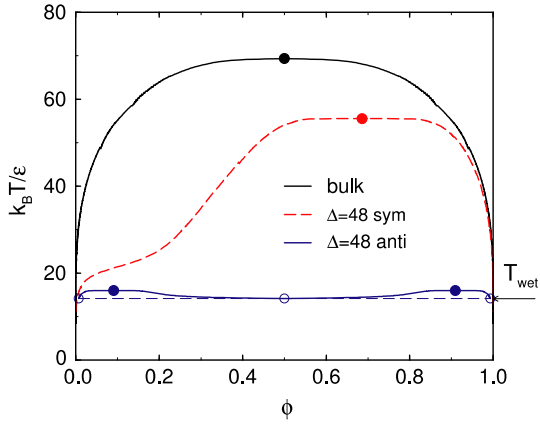

Fig. 3. Phase diagram in terms of composition and temperature for film thickness $\Delta \approx 2.8R_e$ as obtained from simulations. The arrow marks the wetting transition temperature. $\epsilon_{\text{wall}} = 0.16k_BT$ [from Ref. [11]].

Note the pronounced distortion of the B-rich binodal in the vicinity of the wetting transition. In the B-rich phase there are A-rich layers at the surfaces and the B component prevails in the middle of the film. In the vicinity of the wetting transition the thickness of the A-enrichment layers grows as we increase the temperature. If we increased the film thickness, this distortion would evolve into an additional two-phase region [10,23], corresponding to a B-rich phase with thin and thick A-layers at the surface. This two-phase region would correspond to the pre-wetting coexistence and it would join the B-rich binodal in a triple point.

The phase diagram of an antisymmetric film is also presented in Fig. 3. In this case one surface attracts the A-component with exactly the same strength as the other surface, the B-component. The phase diagram contains two critical points and a triple line [8,9,11]. Around the critical temperature of the bulk, enrichment layers gradually form at the surfaces and stabilize an AB interface that runs parallel to the surfaces. At the interface localization/delocalization transition [24–26], this AB interface becomes bound to one of the surfaces. In the case of a first-order interface localization/delocalization transition, this corresponds to a triple point of the phase diagram: an A-rich phase, a B-rich phase, and a phase with symmetric composition coexist.

The behavior can be analyzed qualitatively by looking at the interface potential $g(l)$ which describes the interaction between an AB interface and a single surface. If the film is thick enough, the interface potential

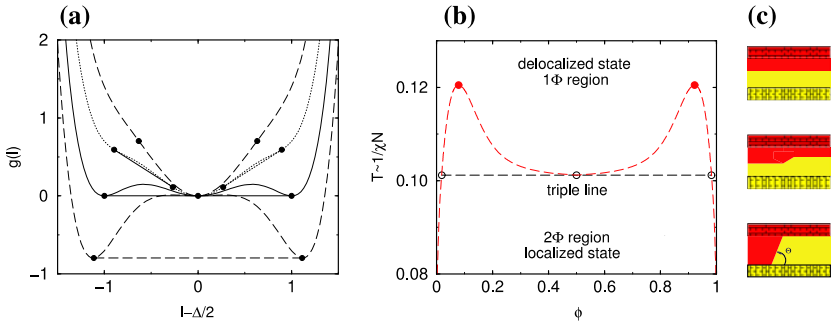

Fig. 4. (a) Schematic temperature dependence of the effective interface potential in a film with antisymmetric surfaces. The temperatures correspond to (from bottom to top) $T < T_{\text{trip}}$, T_{trip}, $T_{\text{trip}} < T < T_c^{\text{film}}$ and T_c^{film}. (b) Phase diagram of a mixture. (c) Sketches of typical configurations for $T > T_c^{\text{film}}$ (upper panel), $T_{\text{trip}} < T < T_c^{\text{film}}$ in the miscibility gap (middle panel) and $T < T_{\text{trip}}$ (lower panel) [from Ref. [12]].

can be constructed as a superposition of the interface potentials emerging from each surface. The qualitative behavior in the vicinity of a first-order wetting transition is depicted in Fig. 4a. Using a double-tangent construction, we can deduce the phase behavior in a thin film. At low temperatures there coexist an A-rich phase and a B-rich phase, in which the AB interface is localized at the surface. Upon increasing the temperature, one encounters the triple point. This triple point is the thin film analog of the first-order wetting transition. As the film thickness increases, the triple temperature converges towards the wetting transition temperature of the semi-infinite system. Above the triple temperature, there are two-phase coexistence regions, which correspond to thin and thick enrichment layers at the surfaces. This is the analog of the pre-wetting transition in a thin film.

4.2. Tricritical Interface Localization/Delocalization Transition

If we reduce the film thickness, the interactions emerging from each surface interfere. The phenomenological considerations [11] explain that this leads to a second-order interface localization/delocalization transition at small film thicknesses. Both regimes are separated by a tricritical transition. The scaled distribution functions prove convenient to locate the tricritical thickness accurately. To this end we have adjusted the temperature such that the central peak of the probability distribution of the order parameter $m \sim \phi_A - \phi_B$ is a factor 1.2 higher than the outer peaks. This corresponds to the behavior of the universal distribution of the 2D

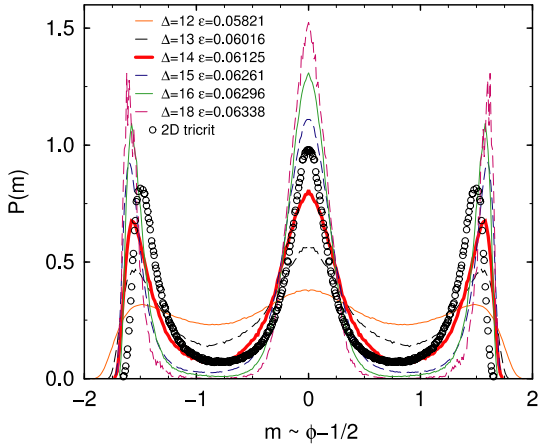

Fig. 5. Probability distribution for various film thicknesses as indicated in the key scaled to unit norm and variance. The lateral system size is $L = 96$. The universal distribution of the 2D tricritical universality class [27] is presented by circles [from Ref. [11]].

tricritical universality class [27]. The results for various film thicknesses Δ (in units of the lattice spacing) are presented in Fig. 5. For $\Delta < \Delta_{\text{tri}}$ the valleys between the three peaks are too shallow (cf. Fig. 5), while they are too deep for $\Delta > \Delta_{\text{tri}}$. In the latter case the transition is of first order and our estimate tends towards the triple temperature. At $\Delta_{\text{tri}} \approx 14 = 0.89 R_e$ the distribution of our simulations is similar to the universal 2DT distribution, and this has been confirmed for larger lateral system sizes [11].

4.3. Crossover from Capillary Condensation to Interface Localization/Delocalization

Realizing strictly (anti)symmetric surface interactions is often difficult in experiments. Varying the surface interaction $\Lambda_2 N$ of the top surface from attracting the A-component to attracting the B-component (while the bottom surface always attracts the A-component with fixed strength $\Lambda_1 N$), we study the crossover from capillary condensation for symmetric surfaces to interface localization/delocalization for antisymmetric surfaces. The dependence of the phase diagram on the surface interactions within the SCF calculations is presented in Fig. 6. For symmetric surfaces (capillary condensation) the critical point is shifted towards lower temperatures [4] similar to the simulation result. Of course, the binodals are parabolic in

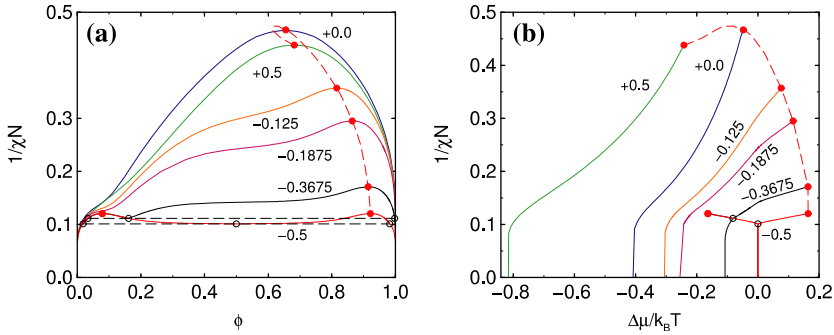

Fig. 6. (a) Binodals for $\Delta_0 = 2.6R_e$ and surface interaction $\Lambda_1 N = 0.5$ obtained from SCF calculations. The surface interaction at the other surface $\Lambda_2 N$ varies as indicated in the key. The dashed curve shows the location of the critical points. Filled circles mark critical points, open circles/dashed horizontal lines denote three–phase coexistence for $\Lambda_2 N = -0.3675$ and -0.5. (b) Coexistence curves in the χN-$\Delta\mu$ plane. The "quasi-pre-wetting" lines for $\Delta\mu < 0$ and $\Lambda_2 N = -0.3675$ and -0.5 are indistinguishable, because they are associated with the pre-wetting behavior of the surface with interaction $\Lambda_1 N = +0.5$ [from Ref. [8]].

mean field theory independent from dimensionality. The coexisting phases have almost uniform composition across the film and differ in their composition. As we reduce the preference of the top surface for species B, the critical point and the critical composition tend towards their bulk values ($\phi = 0.5$, $1/\chi N = 0.5$), i.e., the critical temperature increases and the critical composition becomes more symmetric [8]. The coexistence curve in the $1/\chi N$-$\Delta\mu$ plane approaches the symmetry axis. Upon making the top surface attracting the other component B, we gradually change the character of the phase transition towards an interface localization/delocalization transition [24,25]. The critical temperature passes through a maximum and the critical composition through a minimum. For $\Lambda_2 N < 0$ (surface attracting the B-component) there are enrichment layers of the A-component at the bottom and the B-component at the top, and the two coexisting phases differ in the location of the AB interface which runs parallel to the surfaces. As the preferential interaction of the top surface increases, the critical temperature decreases and the critical composition becomes richer in A. When the coexistence curve intersects the pre-wetting line of the bottom surface at $\Delta\mu < 0$, a triple point forms at which an A-rich phase and two B-rich phases with a thin and a thick A-enrichment layer coexist. When the bottom surface attracts A with exactly the same strength as the top surface B (antisymmetric surfaces), the phase diagram becomes symmetric.

For symmetric surface fields the critical point occurs close to the bulk critical point (and converges towards it in the limit of infinite film thickness) while the critical points in antisymmetric films are associated with the wetting transition and converge towards the pre-wetting critical temperature of the semi-infinite system (if the wetting transition is of first order) for $\Delta \to \infty$. In both cases, however, critical points belong to the 2D Ising universality class.

5. INTERFACE LOCALIZATION/DELOCALIZATION IN AN ANTISYMMETRIC DOUBLE WEDGE

5.1. Background

In the following we consider wetting (or rather filling) in a wedge geometry. Macroscopic considerations show that the wedge will be filled with liquid when the contact angle Θ on a planar substrate equals the opening angle α. Intriguingly, Parry and co-workers [28] predict that the filling of a wedge is related to the strong fluctuation regime of critical wetting and that critical filling may even occur if the concomitant wetting transition of the planar surface is of first order. Specifically, they predicted the distance l_0 of the AB interface from the bottom of a wedge to diverge as $l_0 \sim (T_f - T)^{-\beta_s}$ with $\beta_s = 1/4$. Correlations along the wedge and in the other two directions are characterized by diverging correlation lengths, $\xi_y \sim (T_f - T)^{-\nu_y}$ and $\xi_x \sim \xi_\perp \sim (T_f - T)^{-\nu_\perp}$, with exponents $\nu_y = 3/4$ and $\nu_\perp = 1/4$, respectively.

In the following we study a wedge with an opening angle $\alpha = \pi/4$ of the wedge (c.f. Fig. 7). Similar to the study of wetting, an antisymmetric geometry is advantageous. Therefore, we stack two wedges which attract different components on top of each other. This antisymmetric double wedge is a pore with a quadratic cross section of size $L \times L$. Let L_y denote the length of the wedge (c.f. Fig. 7). (i) If we used identical surface fields on all four free surfaces, the analog of capillary condensation would occur in a wedge, i.e., phase coexistence would be shifted away from the bulk coexistence curve and the wetting layers would be only metastable (with respect to "wedge condensation"). (ii) As the wetting layer grew on all four surfaces in the case of symmetric boundaries, we would need larger system sizes to reduce interactions between the wetting layers across the wedge.

The phase behavior in such an antisymmetric double wedge geometry has been studied recently in the framework of an Ising model [15,16]. When the wetting transition of the planar substrate was of first order, the wedge filling was also found to be of first order. When the wetting transition was of second order, an unconventional scaling behavior was

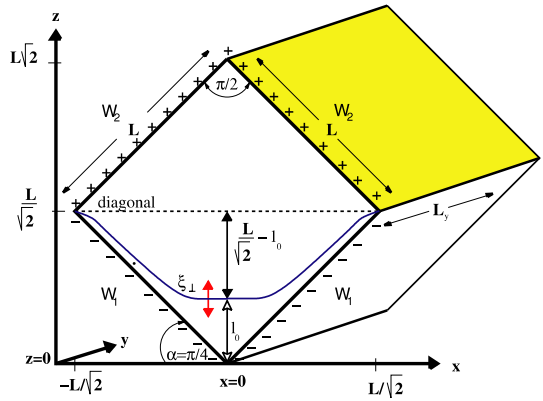

Fig. 7. Antisymmetric double wedge: periodic boundary conditions apply along the y-direction and there are 4 impenetrable surfaces of size $L \times L_y$. The bottom ones (W_1) attract the A-component with strength ϵ_{wall} and the top ones (W_2) attract the B-component. l_0 denotes the position of the interface from one corner [from Ref. [15]].

observed which is characterized by critical exponents $\alpha = 3/4, \beta = 0$, and $\gamma = 5/4$. Those critical exponents can be related (see below) to the exponents of critical wedge filling, and the simulations of the Ising model confirm the predictions of Parry and co-workers [28].

In the following we corroborate these findings in the framework of the Ising model by our polymer simulations. Moreover, we present evidence for the unconventional second-order transition in an antisymmetric double wedge even though the wetting transition on a planar substrate is of first order.

We present preliminary simulation data for two temperatures: $\epsilon/(k_B T) = 0.025$ $(T/T_c = 0.58)$ and $\epsilon/(k_B T) = 0.05$ $(T/T_c = 0.29)$. At both temperatures the wetting transitions, which occur at an appropriate attractive strength ϵ_{wall} of planar surfaces, are of first order (c.f. Fig. 2). In the former case, it is a weak first-order wetting transition; in the latter case, it is a strong first-order transition.

5.2. First-Order Transition in an Antisymmetric Double Wedge

At the lower temperature $\epsilon/(k_B T) = 0.05$, the behavior is similar to a first-order interface localization/delocalization transition. We consider here only the case $\Delta\mu = 0$ where phase coexistence in the bulk occurs. This excludes the rather interesting interplay between pre-wetting and pre-filling behavior studied in Ref. [29]. At large surface interaction $\epsilon_{\text{wall}} > \epsilon_{\text{wall}}^{\text{trip,wedge}}$,

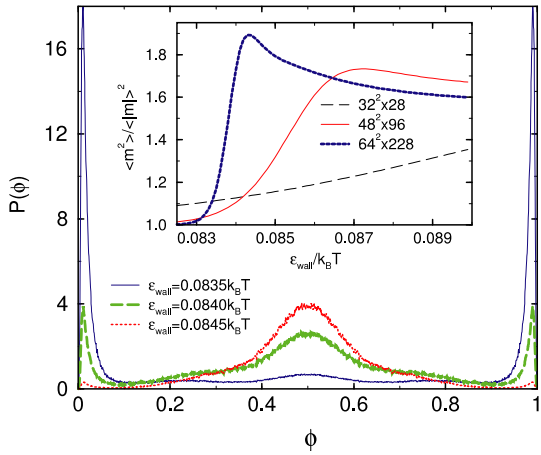

Fig. 8. The probability distribution of the composition at $\epsilon/(k_BT) = 0.05$ and system geometry $64^2 \times 228$ exhibits a three-peak structure, which is characteristic of a first-order transition. The inset shows the dependence of the cumulant $\langle m^2 \rangle / \langle |m| \rangle^2$ with $m \sim \phi - 1/2$ on ϵ_{wall} for three different system sizes.

there runs an AB interface along the diagonal which divides the two double wedges. This corresponds to the delocalized state. Upon decreasing ϵ_{wall} (or decreasing the temperature), the AB interface becomes localized in one of the wedges. In this case the composition of the double wedge is either A-rich or B-rich and we define as order parameter $m \equiv \phi_A - \phi_B$. The two situations are separated by a triple point $\epsilon_{\text{wall}}^{\text{trip,wedge}}$ at which the interface can be localized in either of the wedges or delocalized on the diagonal. The trimodal probability distribution in the vicinity of the tricritical point is presented in Fig. 8. In analogy to the case of antisymmetric films, we expect this triple point in a double wedge to correspond to a first-order filling transition. In the inset we show the cumulant $\langle m^2 \rangle / \langle |m| \rangle^2$. If the transition was of second order, these cumulants would depend monotonically on ϵ_{wall} and would exhibit a common intersection point. This is not at all what we observe, and we conclude that the interface localization/delocalization transition in the double wedge is of first order at the lower temperature $\epsilon/(k_BT) = 0.05$.

5.3. Critical Behavior in an Antisymmetric Double Wedge

Even though the wetting transition on a planar surface at $\epsilon/(k_BT) = 0.025$ is of first order, the behavior at the interface localization/delocalization

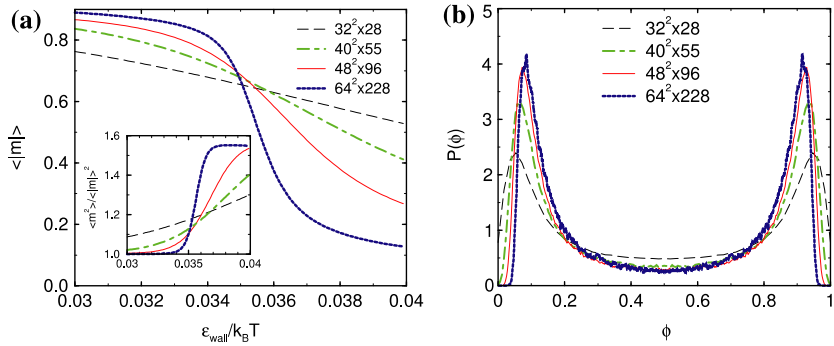

Fig. 9. (a) Dependence of the absolute order parameter $m \equiv |\phi_A - \phi_B|$ on the surface interactions ϵ_{wall} at $\epsilon/(k_B T) = 0.05$. The insert shows the cumulant. (b) Scaling of the probability distribution at $\epsilon_{\text{wall}} = 0.035$ and various system sizes.

transition in an antisymmetric double wedge at high temperature differs from the transition at low temperature. In the inset of Fig. 9a we present the dependence of the cumulant on the surface interaction strength for various system sizes. The cumulants depend monotonically on ϵ_{wall} and exhibit a common intersection point around $\epsilon_{\text{wall}}^{\text{crit}} \approx 0.035$. In Fig. 9b we show the probability distribution of the composition ϕ at this intersection point: the distribution is bimodal, and the two largest system sizes collapse onto a master curve without any size dependent prefactor. Therefore we conclude that the interface localization/delocalization transition is of second order.[5]

Intriguingly there are also marked differences between this second-order transition in an antisymmetric double wedge and the second-order transition in a thin film which belongs to the 2D Ising universality class. In the latter case, only the distribution of the *scaled* order parameter $L^{\beta/\nu}m$, where $\beta = 1/8$ and $\nu = 1$ are the critical exponents of the order parameter and the correlation length in the 2D Ising universality class, exhibits data collapse for different system sizes. Moreover, we present in Fig. 9a the dependence of the absolute value of the magnetization in the vicinity of the transition. Curves for different system sizes exhibit a common intersection point which agrees well with the intersection point of the cumulants. The analogous curves at an Ising-like transition do not exhibit a common

[5] The interface localization/delocalization transition might be of second order in a very thin antisymmetric film (c.f. Section 4.2) even if the wetting transition is of first order. Therefore still larger system sizes would be desirable to confirm this conclusion. We note however, that the thickness of the enrichment layer at the first-order wetting transition of the planar substrate ($\epsilon/(k_B T) = 0.0226, \epsilon_{\text{wall}}^{\text{wet}}/(k_B T) = 0.04$) is only $l_0 \approx 4 \ll 45.2 = L/\sqrt{2}$. Therefore we believe that our conclusion is not affected by finite size effects.

intersection point but monotonically converge towards $\langle |m| \rangle \sim |T - T_c|^{\beta}$ for $T < T_c$ and $\langle |m| \rangle \equiv 0$ for $T \geqslant T_c$ upon increasing the system size.

To relate the critical behavior of the antisymmetric double wedge to the predictions of Parry *et al.* [28], we regard the distance l_0 of the AB interface from the corner of one wedge. Similar to an antisymmetric film (c.f. Section 4.1), we assume that we can approximate the distribution in a double wedge by the superposition of the distributions of single wedges $P_{\text{wedge}}(l_0)$ via $P(l_0) \sim P_{\text{wedge}}(l_0) + P_{\text{wedge}}(\sqrt{2}L - l_0)$ If the two distributions, $P_{\text{wedge}}(l_0)$ and $P_{\text{wedge}}(\sqrt{2}L - l_0)$, do not overlap, the AB interface will be located in either of the two wedges and the order parameter will not vanish. If the two distributions overlap, the interface fluctuates around the diagonal and the order parameter will be zero. Right at the transition the two distributions begin to overlap:

$$\langle l_0 \rangle + \xi_{\perp} \stackrel{!}{=} \sqrt{2}L - \langle l_0 \rangle - \xi_{\perp}$$

(interface localization/delocalization in double wedge) (1)

where $\langle l_0 \rangle$ denotes the mean height in a single wedge and $\xi_{\perp}$ denotes its fluctuations. Importantly, Parry's prediction of $\beta_0 = \nu_{\perp}$ in wedges (and also corners [30]) means that the height and its fluctuations are of the same order. They diverge in the same way as we approach the critical filling transition.

The height of the interface l_0 is related to the order parameter m of the localization/delocalization transition. Therefore, we expect the distribution of the order parameter also to be bimodal. As $l_0 \sim \xi \sim L$ at the transition and the order parameter is a function of l_0/L, the distribution of the order parameter will exhibit two peaks whose positions and widths will not depend on the system size. This is exactly what we observe in Fig. 9**b**. Using this observation and the standard finite size scaling assumption at a second-order phase transition,

$$P(m) \sim L^{\beta/\nu_{\perp}} \tilde{\mathcal{P}}(L^{\beta/\nu_{\perp}} m, L/\xi_{\perp}, L_y/\xi_y) \sim L^{\beta/\nu_{\perp}} \mathcal{P}(L^{\beta/\nu_{\perp}} m, L^{1/\nu_{\perp}} t, \eta) \quad (2)$$

where $\tilde{\mathcal{P}}$ and $\mathcal{P}$ are scaling functions, $t = (T - T_f)/T_f$ denotes the relative distance to the filling transition, and $\eta \equiv L_y / L^{\nu_y/\nu_{\perp}} = L_y/L^3$ denotes the generalized aspect ratio, we conclude $\beta/\nu_{\perp} = 0$. Due to the anisotropy of the fluctuations of the interface along the wedge with correlation length ξ_y and perpendicular to the wedge with correlation length $\xi_{\perp}$, the generalized aspect ratio appears as a scaling variable. In our simulations we have chosen the system geometry such that η remains approximately constant to ensure that finite-size rounding in the direction along the wedge and the rounding

in the two other directions set in simultaneously.[6] Hence, the scaling of the probability distribution not only confirms $\beta = 0$ but also $\nu_y = 3\nu_\perp$.

Knowing the probability distribution of the order parameter, we can calculate all its moments:

$$\langle m^k \rangle = \mathcal{M}_k(L^{1/\nu_\perp} t, \eta) \tag{3}$$

where $\mathcal{M}_k$ are scaling functions. As a special case, we calculate the susceptibility: $\chi = L^2 L_y \langle m^2 \rangle / k_B T \sim L^2 L_y \tilde{\mathcal{M}}_2(L/\xi_\perp, L_y/\xi_y) \sim \xi_\perp^2 \xi_y \sim t^{-2\nu_\perp - \nu_y} \equiv t^{-\gamma}$ with $\gamma = 2\nu_\perp + \nu_y = 5/4$. Gratifyingly, these values for the exponents comply with the anisotropic hyperscaling relation [31], $\gamma + 2\beta = (d-1)\nu_\perp + \nu_y$. Using thermodynamic scaling $2 - \alpha = \gamma + 2\beta$, we infer the critical exponent $\alpha = 3/4$ for the specific heat. Another consequence of the absence of any L-dependent prefactor in Eq. (3) is the common intersection of moments of the order parameter at the transition. Again this is an agreement with our observation in Fig. 8**a**. As this intersection involves only the lowest moment of the order parameter, it yields an accurate estimate of the location of the critical interface localization/delocalization transition in an antisymmetric double wedge.

It is interesting to relate the observation of first- and second-order interface localization/delocalization transitions in a double wedge to the shape of the interface potential. Parry *et al.* [28] predict that the filling transition is second order if the interface potential between an AB interface and a planar surface does not exhibit a free energy barrier between the minimum close to the surface and the behavior at large distances, i.e., if a macroscopically thick film is not even metastable.

In Fig. 10 we present the interface potential obtained from the probability distribution of the composition in a simulation of an antisymmetric film at $\epsilon/(k_B T) = 0.025$. In the vicinity of the wetting transition the interface potential exhibits a maximum between the minimum close to the surface and the value at large distances. This fact confirms that the wetting transition is of first order. At the smaller value of ϵ_{wall}, however, there is no such maximum within the statistical uncertainty of the Monte Carlo data and, in agreement with Parry's predictions, we observe a second-order transition in the double wedge.

[6] If we kept the ratio L_y/L constant $\eta \to 0$ and the system would exhibit a behavior characteristic of a corner. In the limit L fixed but $L_y \to \infty$ the wedge becomes quasi-one-dimensional and there is no transition [16].

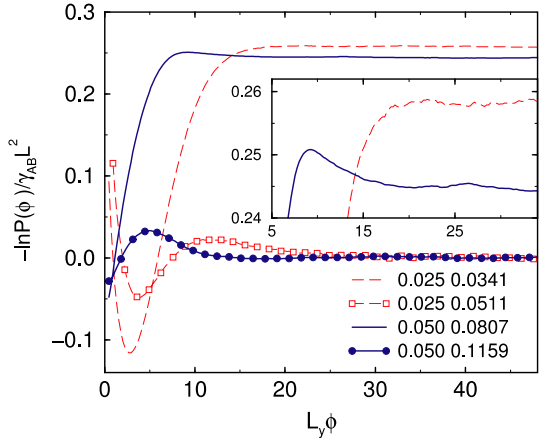

Fig. 10. The probability distribution of the composition in an antisymmetric film with system geometry $48^2 \times 96$. Values of $\epsilon/(k_BT)$ and $\epsilon_{\text{wall}}/(k_BT)$ (shown in the key) correspond to the wetting transition and the filling transition (according to Young's equation). The inset presents an enlarged view of the same graph ($-\ln P(\phi)\gamma_{AB}L^2$ *vs.* $L_y\phi$) for the filling transitions at high (dashed line) and low (solid line) temperatures. The maximum of the interface potential indicates that the filling transition is of first order at low temperatures, and its absence is the hallmark of a second-order filling transition at high temperatures. Note that the wetting transition is of first order at both temperatures.

6. SUMMARY

We have investigated the interplay between wetting and phase separation of incompressible binary mixtures confined in thin films and wedges. In our polymer model the wetting transition is of first order and we can accurately locate it via Young's equation. The concomitant pre-wetting behavior modifies the phase boundaries in thin films. If both surfaces attract the same component, capillary condensation occurs and the critical point is close to the critical unmixing transition in the bulk. If one surface attracts the A-component but the other attracts the B-component, an interface localization/delocalization transition occurs. In this case there are two critical points which correspond to the pre-wetting critical points at each surface. If the film thickness is very small, however, the interface localization/delocalization transition might be of second order even if the wetting transition is of first order. The critical points in a thin film are characterized by Ising critical behavior.

In analogy to the interface localization/delocalization in an antisymmetric film, we have studied the transition in an antisymmetric double wedge and we relate the phase behavior to the filling transition in a single wedge. Importantly, we present evidence that the analog of critical filling in an antisymmetric double wedge geometry gives rise to unconventional critical behavior characterized by an order parameter exponent $\beta = 0$ and strong anisotropic fluctuations [15]. We can relate the critical exponents to the predictions of Parry *et al.* [28] on critical filling. In agreement with those predictions the filling transition can be critical even though the wetting transition on a planar substrate is of first order. This is practically important because there is no experimental realization of critical wetting on a solid substrate. Our findings suggests the polymer blends might be promising candidates to explore the filling behavior experimentally.

ACKNOWLEDGMENTS

It is a great pleasure to thank E. V. Albano, D. P. Landau, and A. Milchev for fruitful collaborations and A. O. Parry for stimulating discussions. Financial support by the DFG under grants Mu 1674/3-1, Bi314/17-4, and DAAD/PROALAR 2000 as well as computer time at NIC Jülich and HLR Stuttgart are acknowledged.

REFERENCES

1. S. Dietrich, *Phase Transitions and Critical Phenomena*, Vol. 12, C. Domb and J. Lebowitz, eds. (Academic Press, London, 1988); M. Schick, in *Liquids at Interfaces*, J. Charvolin, J. F. Joanny, and J. Zinn-Justin, eds. (North Holland, Amsterdam, 1990), p. 415.
2. R. Evans, *J. Phys.: Condens. Matter* **2**:8989 (1990).
3. A. O. Parry, *J. Phys.: Condens. Matter* **8**:10761 (1996).
4. M. E. Fisher and H. Nakanishi, *J. Chem. Phys.* **75**:5857 (1981); H. Nakanishi and M. E. Fisher, *J. Chem. Phys.* **78**:3279 (1983).
5. L. D. Gelb, K. E. Gubbins, R. Radhakrishnan, and M. Sliwinska-Bartkowiak, *Rep. Prog. Phys.* **62**:1573 (1999).
6. J. Rysz, A. Budkowski, A. Bernasik, J. Klein, K. Kowalski, J. Jedlinski, and L. J. Fetters, *Europhys. Lett.* **50**:35 (2000).
7. M. Geoghegan, H. Ermer, G. Jüngst, G. Krausch, and R. Brenn, *Phys. Rev.* **E 62**:940 (2000).
8. M. Müller, K. Binder, and E. V. Albano, *Europhys. Lett.* **49**:724 (2000).
9. M. Müller, E. V. Albano, and K. Binder, *Phys. Rev.* **E 62**:5281 (2000); M. Müller, K. Binder, and E. V. Albano, *Physica* **A 279**:188 (2000).
10. M. Müller and K. Binder, *Macromolecules* **31**:8323 (1998).
11. M. Müller and K. Binder, *Phys. Rev.* **E 63**:021602 (2001).
12. M. Müller, K. Binder, and E. V. Albano, *Int. J. Mod. Phys.* **B15**:1867 (2001).
13. M. Müller, *Macromol. Theory Simul.* **8**:343 (1999).
14. I. Carmesin and K. Kremer, *Macromolecules* **21**:2819 (1988).

15. A. Milchev, M. Müller, K. Binder, and D. P. Landau, *Phys. Rev. Lett.* **90**:131601 (2003).
16. A. Milchev, M. Müller, K. Binder, and D. P. Landau, *Phys. Rev. E* **68**:031601 (2003)
17. M. Müller, *Comp. Phys. Comm.* **147**:292 (2002).
18. T. Geisinger, M. Müller, and K. Binder, *J. Chem. Phys.* **111**:5241 (1999).
19. T. Young, *Phil. Trans. Roy. Soc.* (*London*) **95**:65 (1805).
20. M. Müller and L. G. MacDowell, *Macromolecules* **33**:3902 (2000).
21. I. Carmesin and J. Noolandi, *Macromolecules* **22**:1689 (1989).
22. A. N. Semenov, *J. Phys. II* (*France*) **6**:1759 (1996).
23. D. Nicolaides and R. Evans, *Phys. Rev.* **B 39**:9336 (1989).
24. F. Brochard–Wyart and P.-G. de Gennes, *Acad. Sci. Paris* **297**:223 (1983).
25. A. O. Parry and R. Evans, *Phys. Rev. Lett.* **64**:439 (1990), Physica **A 181**:250 (1992).
26. K. Binder, D. P. Landau, and A. M. Ferrenberg, *Phys. Rev.* **E 51**:2823 (1995).
27. N. B. Wilding and P. Nielaba, *Phys. Rev.* **E 53**:926 (1996).
28. A. O. Parry, C. Rascon, and A. J. Wood, *Phys. Rev. Lett.* **83**:5535 (1999).
29. K. Rejmer, S. Dietrich, and M. Napiorkowski, *Phys. Rev.* **E 60**:4027 (1999).
30. E. V. Albano, A. de Virgiliis, M. Müller, and K. Binder, *J. Phys.: Condens. Matter* **15**:333 (2003).
31. K. Binder and J. S. Wang, *J. Stat. Phys.* **55**:87 (1989).